Cancer Research

Enhancement of Antitumor Immunity in Lung Cancer by Targeting Myeloid-Derived Suppressor Cell Pathways

Anandi Sawant[1], Cara C. Schafer[2], Tong Huan Jin[2], Jaroslaw Zmijewski[2], Hubert M. Tse[3], Justin Roth[4], Zhihuan Sun[2], Gene P. Siegal[1], Victor J. Thannickal[2], Stefan C. Grant[2], Selvarangan Ponnazhagan[1], and Jessy S. Deshane[2]

Abstract

Chemoresistance due to heterogeneity of the tumor microenvironment (TME) hampers the long-term efficacy of first-line therapies for lung cancer. Current combination therapies for lung cancer provide only modest improvement in survival, implicating necessity for novel approaches that suppress malignant growth and stimulate long-term antitumor immunity. Oxidative stress in the TME promotes immunosuppression by tumor-infiltrating myeloid-derived suppressor cells (MDSC), which inhibit host protective antitumor immunity. Using a murine model of lung cancer, we demonstrate that a combination treatment with gemcitabine and a superoxide dismutase mimetic targets immunosuppressive MDSC in the TME and enhances the quantity and quality of both effector and memory $CD8^+$ T-cell responses. At the effector cell function level, the unique combination therapy targeting MDSC and redox signaling greatly enhanced cytolytic $CD8^+$ T-cell response and further decreased regulatory T cell infiltration. For long-term antitumor effects, this therapy altered the metabolism of memory cells with self-renewing phenotype and provided a preferential advantage for survival of memory subsets with long-term efficacy and persistence. Adoptive transfer of memory cells from this combination therapy prolonged survival of tumor-bearing recipients. Furthermore, the adoptively transferred memory cells responded to tumor rechallenge exerting long-term persistence. This approach offers a new paradigm to inhibit immunosuppression by direct targeting of MDSC function, to generate effector and persistent memory cells for tumor eradication, and to prevent lung cancer relapse. *Cancer Res; 73(22); 6609–20. ©2013 AACR.*

Introduction

Lung cancer is the primary cause of cancer-related death in both men and women with an overall 5-year survival rate of 15% (1, 2). Current first-line therapies often involve chemotherapeutic combinations that target the heterogeneity of signaling pathways active among malignant cell populations. Nevertheless, chemoresistance of tumor cells continues to pose a significant challenge for these strategies to be efficacious in prolonging patient survival. Hence, multimodal therapies that also stimulate antitumor immune responses are essential for long-term management of this disease (3).

Oxidative stress, resulting from elevated reactive oxygen species (ROS), is implicated in the initiation and progression of lung cancer (4). The host protective antitumor immunity is also often suppressed by several nonmalignant leukocyte lineages in the tumor microenvironment (TME), which significantly dampen the long-term efficacy of existing combination therapies for lung cancer (5, 6). Myeloid-derived suppressor cells (MDSC) generate ROS, associated free radicals, and immunoregulatory cytokines to suppress host $CD4^+$ and $CD8^+$ T-cell responses, thereby promoting tumor progression and metastasis (7–9). In patients with advanced stages of lung cancer, increased numbers of circulating MDSC correlate with immunosuppression and enhanced tumor burden (10). Despite the documented roles of these immunosuppressive cells in lung cancer, few immunomodulatory therapies have been successful at targeting MDSC to enhance long-term immunity. Development of treatment resistance following gemcitabine (Gem) therapy and elevation of ROS in the TME may impact infiltrating immune effector function, induce MDSC proliferation, and impair memory response, which is a critical component of protective immunity. We hypothesized, therefore, that a timely uncoupling of the MDSC-induced immunosuppression in the TME and ROS would not only enhance effects of gemcitabine, but also reactivate host antitumor immunity including both effector and memory functions and significantly enhance survival outcomes.

Herein, we report an innovative therapeutic strategy that both impairs MDSC function and induces effective memory

Authors' Affiliations: Departments of [1]Pathology, [2]Medicine, [3]Microbiology, and [4]Pediatrics, The University of Alabama at Birmingham, Birmingham, Alabama

Note: Supplementary data for this article are available at Cancer Research Online (http://cancerres.aacrjournals.org/).

Corresponding Author: Jessy S. Deshane, Department of Medicine, Division of Pulmonary, Allergy and Critical Care Medicine, 1900 University Boulevard, THT-433, University of Alabama at Birmingham, Birmingham, AL 35294. Phone: 205-996-2041; Fax; 205-934-1721; E-mail: treena@uab.edu

doi: 10.1158/0008-5472.CAN-13-0987

T-cell responses against lung tumors. Using a syngeneic lung cancer mouse model, we demonstrate that gemcitabine, a well-established chemotherapy agent for lung cancer and a known inhibitor of MDSC expansion, along with superoxide dismutase mimetic (SOD mim), reduced tumor growth and resulted in long-term immunity and survival. This combination therapy enhanced the quantity and quality of the effector and memory $CD8^+$ T-cell responses with an enrichment of self-renewing memory cells. Cellular redox–mediated regulation of STAT-3 activation and metabolism of the central memory and effector memory $CD8^+$ T cells contributed to the long-term immunity. Furthermore, adoptive transfer experiments demonstrated that inhibition of MDSC and MDSC-generated ROS enhanced the persistence of memory $CD8^+$ T cells, as well as their vigorous activity in response to reencountering tumor antigens as in stages of relapse. This study clearly delineates the role of MDSC in lung cancer progression and demonstrates utility of this combination therapy for inhibiting tumor and MDSC expansion, abrogating their key molecular functions/pathways and offers a new strategy for treatment of early lung cancer and prevention of relapse.

Materials and Methods

Syngeneic orthotopic lung cancer model

The murine Lewis Lung carcinoma (LLC) cell line (American Type Culture Collection) was propagated in Dulbecco's Modified Eagle Medium (DMEM) supplemented with 10% FBS, 1 mmol/L sodium pyruvate, 2 mmol/L L-glutamine, 10 μg/mL penicillin—streptomycin, and 0.1 mmol/L nonessential amino acids (Life Technologies). LLC cells (10^6) were injected either intravenously, via tail-vein or via an intracardiac route in syngeneic, 6- to 8-week-old female C57BL/6 mice (Frederick Cancer Research and Development Center, Frederick, MD). Analyses included assessment of tumor growth and survival. Tumors, lungs, and spleen tissues were used for enumeration and characterization of MDSC, regulatory T cells (Treg), and $CD8^+$ T-cell memory subsets.

In vivo treatment regimen

LLC-challenged mice were treated with gemcitabine and a SOD mim either individually or in combination (see the treatment model in Fig. 2). Five days after tumor challenge via an intravenous route and 3 days after tumor challenge via an intracardiac route, mice were injected intraperitoneally with either PBS or 60 mg/kg gemcitabine (Sigma-Aldrich) in 50 μL/mouse and 10 mg/kg SOD mim [MnTE-2-PyP^{5+} (manganese (III) mesotetrakis (di-*N*-diethylimidazole) porphyrin], generously provided by Dr. James Crapo (National Jewish Hospital, Denver, CO), in 100 μL/mouse, twice in the first week and once in the following week. Alternatively, LLC-challenged mice received anti-Gr1 antibody (250 μg/100 μL; ref. 11) or immunoglobulin G (IgG) control (BioXCell) intraperitoneally at day 5 either individually or in combination with SOD mim. Catalase-deficient mice (a kind gift from Dr. Jaroslaw Zmijewski, The University of Alabama at Birmingham, Birmingham, AL) were also challenged with tumor and treated as described above.

Isolation of immune cells and FACS analysis

Infiltrating leukocytes were isolated from minced tumor and lung tissues from LLC-challenged mice by incubation in DMEM containing collagenase-B (2 mg/mL; Roche) and DNase I (0.02 mg/mL; Sigma Chemical) at 37°C for 30 minutes. This was followed by the addition of an equal volume of complete DMEM containing 10% FBS (see Supplementary Methods for additional details). ROS^+ cells in tumor tissues were detected by flow cytometry as described before (12). To quantitate the percentage of apoptotic cells, $CD8^+$ T cells from the tumor tissue were stained by a FITC–Annexin V Apoptosis Detection Kit (BD Biosciences). A total of 50×10^3 events were collected for all analyses using the BD LSRII cytometer (BD Biosciences) and the data were analyzed using FlowJo software.

Immunofluorescence microscopy

Detailed procedures for detection of MDSC and $CD8^+$ T cells in snap-frozen tumor tissues are provided in the Supplementary Methods.

Cytotoxicity assay

$CD8^+$ T-cell memory subsets and effector cells were isolated from LLC-challenged mice with gemcitabine and SOD mim treatment as reviewed previously and then used as the effector cells (E). LLC cells were used as the target population (T). The assay was set up with E:T ratios of 5:1, 10:1, 20:1, and 40:1. The cytotoxicity assay was performed using the LIVE/DEAD Cell-Mediated Cytotoxicity Kit (Molecular Probes). $DiOC_{18}{}^+PI^+$ cells were identified as dead target cells and $DiOC_{18}{}^+PI^-$ cells were identified as live target cells by flow cytometry analysis. The percentage of cytotoxicity was calculated following the manufacturer's guidelines as $[(\text{Dead Cells/Live Cells})_{+\text{effectors}} - (\text{Dead Cells/Live Cells})_{-\text{effectors}}] \times 100$.

Detection of thiols

Cell surface thiols on $CD8^+$ T cells from tumor tissues of LLC-challenged mice treated with gemcitabine and SOD mim were detected by staining with 5 μmol/L Alexa Fluor 633–coupled maleimeide (ALM-633; Life Technologies) for 15 minutes on ice, washed with PBS, and analyzed by flow cytometry.

Metabolomic analysis

$CD8^+$ T-cell memory cell subsets were immunopurified from tumor tissues of LLC-challenged mice following treatment as described above. Cells (100 mg wet weight) were rinsed with ice-cold, isotonic PBS twice and the cell pellet was resuspended in cold methanol (−45°C in dry ice). The methanol slurry was then transferred to a cooled centrifuged tube and centrifuged at 14,000 rpm at −20°C for 10 minutes. The methanol extracts were evaporated to dryness, derivatized, and reconstituted in 100 μL of water before analysis. Metabolites that contain an aldehyde or a ketone in their structure were derivatized using Amplifex (Applied Biosystems). Liquid chromatography/mass spectrometry-multiple reaction monitoring (LC/MS-MRM) analysis was then carried out with the mass spectrometer operating in both the positive and negative modes. Addition of Amplifex adds an amine group to the carbonyl of the ketone/aldehyde, which increases the mass of

the compound by 115 amu. The LC system was reverse-phase with the mobile phase A of 0.1% HCOOH in water and mobile phase B of methanol + 0.1% HCOOH. A Synergi Hydro-RP C18 column, 2 mm × 250 mm was used for analysis.

Phospho-STAT3 flow cytometry and ELISA

Detailed procedures for detection and quantitation of p-STAT-3 activation in $CD8^+$ T-cell memory cell subsets are provided in the Supplementary Methods.

Isolation of $CD8^+$ T-cell memory populations and adoptive transfer

Detailed procedures for characterization, purification, and *in vitro* expansion of $CD8^+$ T-cell memory populations are provided in the Supplementary Methods.

Statistical analysis

Data are represented as mean ± SD. One-way ANOVA with Tukey multiple comparison posttest and the Student *t* test was used for statistical comparisons using GraphPad Prism 5. Statistical significance was determined at the <0.05 level (*, $P < 0.05$; **, $P < 0.01$; and ***, $P < 0.001$). Kaplan–Meier method was used for evaluation of survival patterns in tumor-bearing mice. Results were ranked according to the Mantel–Cox log-rank test and $P < 0.05$ was considered statistically significant. Survival was defined as time until death of mice due to excess tumor burden.

Results

MDSC are elevated with a concomitant decrease in $CD8^+$ T cells during progression of lung cancer

For delineating the role of MDSC in progression of lung cancer, a murine lung cancer model was established by intravenous injection of LLC cells (10^6 cells) in syngeneic C57BL/6 mice. A significant increase in tumor burden was observed by 15 days following *in vivo* establishment and progression of lung cancer (Fig. 1A and B; $P < 0.001$ compared with early-stage tumor burden).

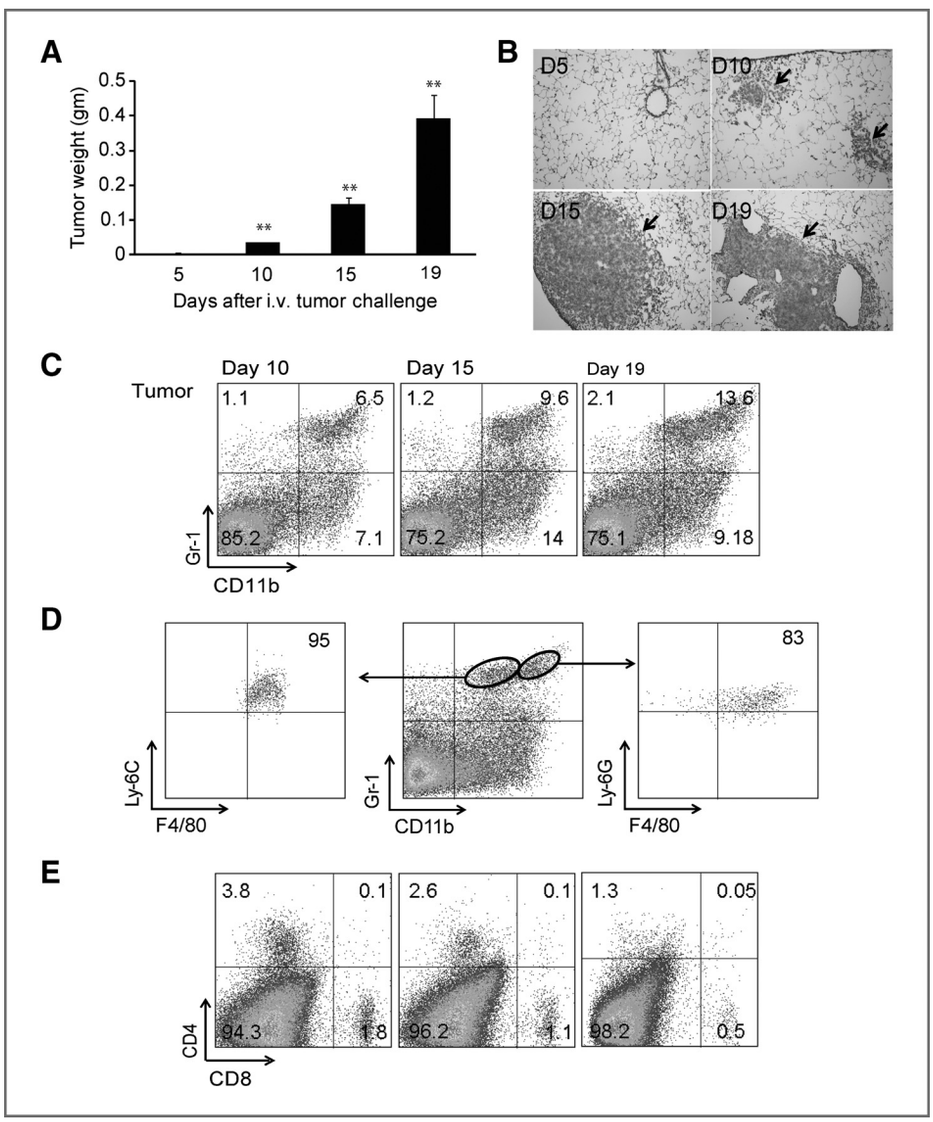

Figure 1. Recruitment of MDSCs were increased, whereas the infiltration of $CD8^+$ and $CD4^+$ T cells were decreased with tumor progression. A, tumor weights from mice on days 5, 10, 15, and 19 after intravenous challenge with 10^6 LLC tumor cells. **, $P < 0.001$ in comparisons with day 5 and 10 compared with day 5 and 15 compared with day 10 and 19 compared with day 15 ($n = 5$ mice/time point, three replicate experiments). B, hematoxylin and eosin staining of lung tissue at indicated time points. C, FACS plots showing percentages of MDSC in tumor on days 10, 15, and 19 post-LLC injection, $P < 0.01$ for $Gr\text{-}1^+CD11b^+$ MDSC at day 19 versus day 15 and for day 10 versus day 15. D, characterization of MDSC subsets by flow cytometry using additional MDSC markers Ly-6C, Ly-6G, and F4/80. E, FACS plots showing $CD8^+$ and $CD4^+$ T cells in tumor at indicated times. Left to right, $P < 0.05$ for both $CD4^+$ and $CD8^+$ T cells, day 10 versus day 15 versus day 19 ($n = 5$ mice/time point, three replicate experiments). The percentages displayed on FACS plots are from a representative run.

We first investigated the progression of tumor growth in the lungs and the significance of infiltrating immunosuppressive cells in the TME. Enumeration of immune cell phenotypes by flow cytometry demonstrated an increase in tumor-infiltrating MDSC with increasing tumor growth (Fig. 1C). The $CD11b^{int}Gr\text{-}1^{int}$ MDSC population stained positive for both Ly-6C and F4/80 (markers characteristic of monocytic phenotype of MDSC), whereas the $CD11b^{hi}Gr\text{-}1^{hi}$ MDSC population expressed both Ly-6G and F4/80 (markers characteristic of granulocytic phenotype of MDSC; Fig. 1D). These MDSC subsets were also characterized in lung and spleen (Supplementary Fig. S1). As the numbers of MDSC increased with tumor burden, a significant reduction in $CD8^+$ and $CD4^+$ T cells was observed (Fig. 1E, same time points as Fig. 1C; $P < 0.05$ with increased tumor growth). Similar enhanced infiltration of MDSC and a steady decline in $CD8^+$ T cells with tumor progression was also noted following intracardiac implantation of tumor cells (Supplementary Fig. S1C).

Treatment of tumor-bearing mice with gemcitabine and a SOD mim targets MDSC and reduces tumor progression

MDSC are negative regulators of protective antitumor immune responses in cancer (7, 8) and use ROS as their primary mechanism for immunosuppression. Therefore, we used gemcitabine, a current first-line chemotherapy for lung cancer, to preferentially target and deplete proliferating MDSC (13–15) in combination with a SOD mim (16, 17) a metalloporphyrin catalytic antioxidant that scavenges ROS in the TME (see treatment model in Fig. 2A). As shown in Fig. 2B, combination therapy of SOD mim + Gem, significantly prolonged the survival of tumor-bearing mice compared with control and individual treatment groups ($P < 0.01$ for Gem vs. SOD mim + Gem, $P < 0.001$ for PBS vs. SOD mim + Gem, $P < 0.001$ for SOD mim vs. SOD mim + Gem). In addition, reduced tumor burden correlated with increased survival (Supplementary Fig. S2B).

A significant reduction in tumor-infiltrating MDSC numbers was noted following combination therapy compared with all other treatment groups (Fig. 2C; $P < 0.01$), with similar observations in lung and spleen tissues (Supplementary Fig. S2A). Furthermore, ROS levels associated with MDSC and other ROS-contributing immune cell types including tumor-associated macrophages (TAM) and tumor-associated neutrophils (TAN) were significantly reduced in the combination therapy group as compared with the PBS control group (Fig. 2D, $P < 0.01$ for ROS^+ MDSC and non-MDSC cells), reflecting an overall reduction of total ROS in TME. Although we observed a significant reduction in tumor-infiltrating neutrophils (Supplementary Fig. S3A), macrophage infiltration was not modulated by combination therapy.

MDSC may also induce development and migration of Tregs to the TME, which can then inhibit antitumor responses and contribute to immunologic tolerance in cancer (18). As shown in Fig. 2E, combination therapy of SOD mim + Gem also significantly reduced the infiltration of Treg ($P < 0.05$).

Combination therapy with a SOD mim and gemcitabine enhances the $CD8^+$ T-cell response

ROS-mediated inhibition of $CD8^+$ T-cell response is the primary immunosuppressive mechanism of MDSC (19, 20). Because increased MDSC infiltration was associated with a reduction of $CD8^+$ T cells during tumor progression, we investigated whether depleting MDSC with combination therapy would modulate the $CD8^+$ T-cell response. The total percentages and absolute numbers of $CD8^+$ T cells increased in tumor, lung, and spleen tissues of mice treated with SOD mim + Gem (Fig. 3A and B) Immunohistochemical analysis further showed a significant increase in the infiltration of $CD8^+$ T cells and a decrease in infiltration of $Gr\text{-}1^+$ cells in the periphery as well as center of tumor tissue in mice treated with combination therapy as compared with controls (Fig. 3C). Furthermore, the combination therapy significantly reduced the percentages of apoptotic $Annexin^+$ $CD8^+$ T cells (Fig. 3D; $P < 0.001$ in comparison with all other treatments and control groups).

Combination therapy enhances the memory $CD8^+$ T-cell response

The effectiveness of $CD8^+$ T cells to tumor challenge is dependent on the state of their differentiation. We investigated whether the increased $CD8^+$ T-cell viability and cell numbers following targeted depletion of MDSC and ROS pathways reflected an increased differentiation into various effector and memory subsets. As shown in Fig. 4A, a significant and rapid increase in the percentages of effector (T_{EM}), central (T_{CM}), and stem cell (T_{SCM}) memory $CD8^+$T cells was observed with tumor progression ($P < 0.001$ for SOD mim + Gem vs. Gem for T_{EM} and T_{SCM}). At 14 days after tumor establishment and 6 to 7 days after therapy, T_{EM} and T_{SCM} subsets were observed in increased numbers. However, the pool of $CD8^+$ memory subsets changed 72 hours later, with significantly higher percentages of all three subsets (Fig. 4B; $P < 0.01$ for SOD mim + Gem vs. Gem for T_{EM} and T_{SCM}; $P < 0.05$ for the same comparison for T_{CM}). Increased T_{EM} levels were also observed in the group treated with only gemcitabine. Further characterization of $CD8^+$ T cells indicated that they expressed stem cell antigen-1 (Sca-1; Fig. 4C; $P < 0.001$ for SOD mim + Gem compared with Gem and PBS; $P < 0.01$ for SOD mim vs. Gem; ref. 21), a marker found on self-renewing $CD8^+$ T cells capable of generating central and effector memory populations. Coexpression of high CD62L expression defined these cells as T_{SCM} as shown in Fig. 4D. The combination therapy, however, did not directly affect the viability of $CD4^+$ or $CD8^+$ T cells *ex vivo* (data not shown). Enhanced $CD8^+$ memory T-cell response was also noted following anti-Gr-1 monoclonal antibody (mAb)–mediated depletion of MDSC and targeting MDSC function with SOD mim (Supplementary Fig. S3B). We did not observe any enhanced targeting effects of SOD mim on LLC tumor cells *in vitro* as pretreatment of LLC tumor cells with increasing concentrations of SOD mim did not sensitize the cells further to treatment with gemcitabine (Supplementary Fig. S3C). Combination treatment also reduced MDSC infiltration and ROS levels in the TME of catalase-deficient mice, which normally have elevated ROS levels. In addition, it reduced the

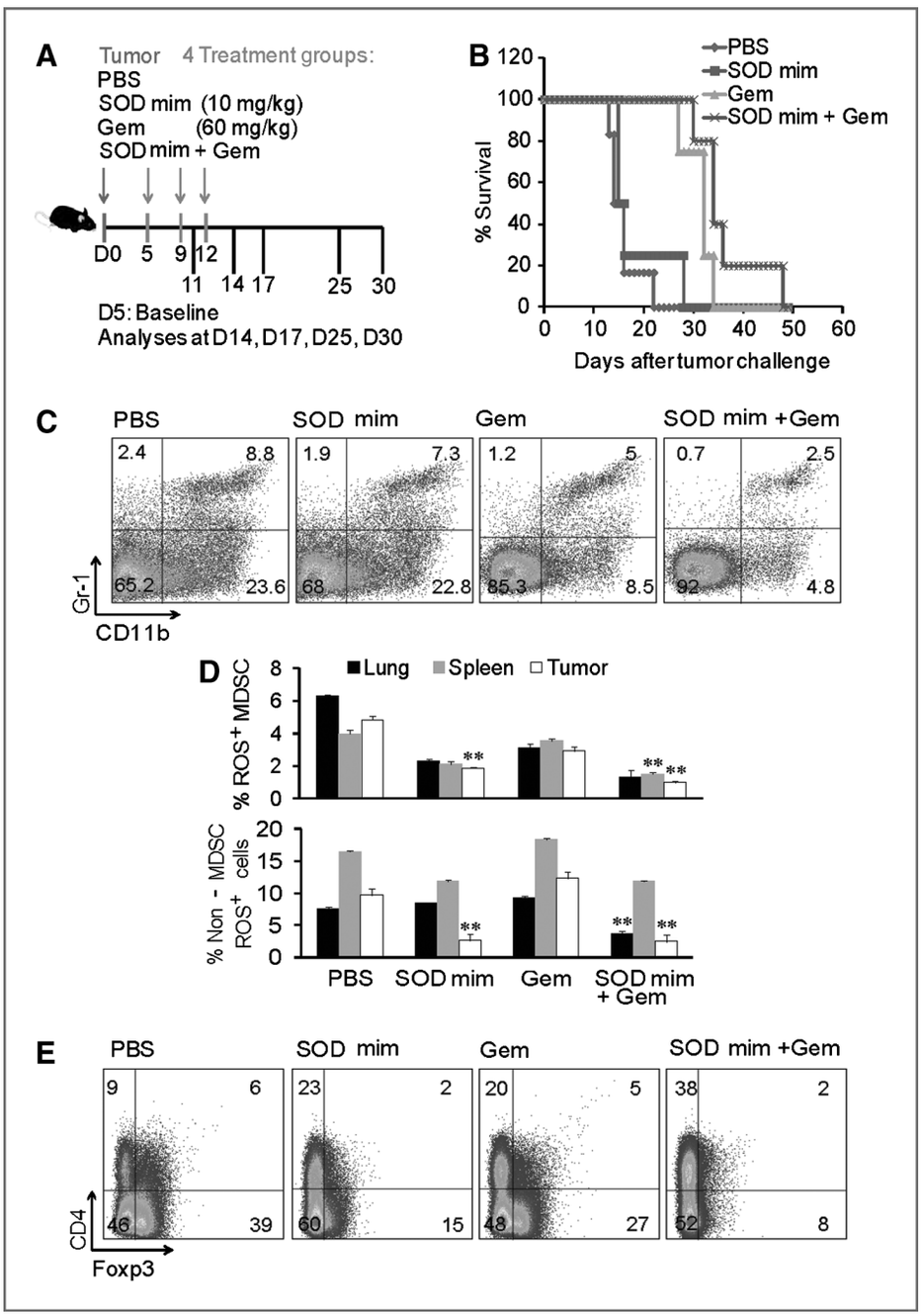

Figure 2. Combination therapy targeted MDSC recruitment efficiently and prolonged survival of mice by reducing tumor burden. A, our model depicting the time-line of tumor challenge, therapy, and analysis. B, Kaplan–Meier survival curve displaying percentage survival among treatment groups after tumor challenge and treatment ($n = 6$ mice/group). Statistical significance was determined by Mantel–Cox log-rank test ($P < 0.05$ for PBS versus SOD mim; $P < 0.001$ for PBS versus Gem; $P < 0.001$ for PBS versus SOD mim + Gem; $P < 0.01$ for Gem versus SOD mim + Gem; $P < 0.001$ for SOD mim versus SOD mim + Gem; and $P < 0.001$ for SOD mim versus Gem). C, FACS plot showing Gr-1$^+$CD11b$^+$ MDSC infiltration in tumor, lung, and spleen of mice from all four treatment groups; $P < 0.01$ for MDSC in treatment groups SOD mim + Gem versus Gem; for comparisons of treatment groups Gem versus SOD mim and for all three treatments compared with PBS controls ($n = 4$ mice/group, four replicate experiments). D, percentage ROS$^+$ MDSC and non-MDSC populations were detected by dihydroethidium (an indicator of ROS) by flow cytometry within the lung, spleen, and tumor tissues for mice from all the four treatment groups. Percentage of ROS$^+$ MDSC in tumor samples: **, $P < 0.01$ for comparisons of treatment groups SOD mim + Gem versus Gem, SOD mim versus PBS, and *, $P < 0.05$ SOD mim versus Gem; spleen samples: **, $P < 0.01$ SOD mim + Gem versus Gem. Percentage of non-MDSC ROS$^+$ cells in tumor samples: **, $P < 0.01$ for SOD mim and SOD mim + Gem versus Gem; lung samples: **, $P < 0.01$ SOD mim + Gem compared with SOD mim, Gem, and PBS groups. E, representative FACS plots showing percentage of CD4$^+$FoxP3$^+$ cells in tumor tissues of mice from all the treatment groups; *, $P < 0.05$ for CD4$^+$FoxP3$^+$ cells in comparisons of SOD mim + Gem and SOD mim versus Gem and PBS controls. The percentages displayed on all FACS plots are from a representative run.

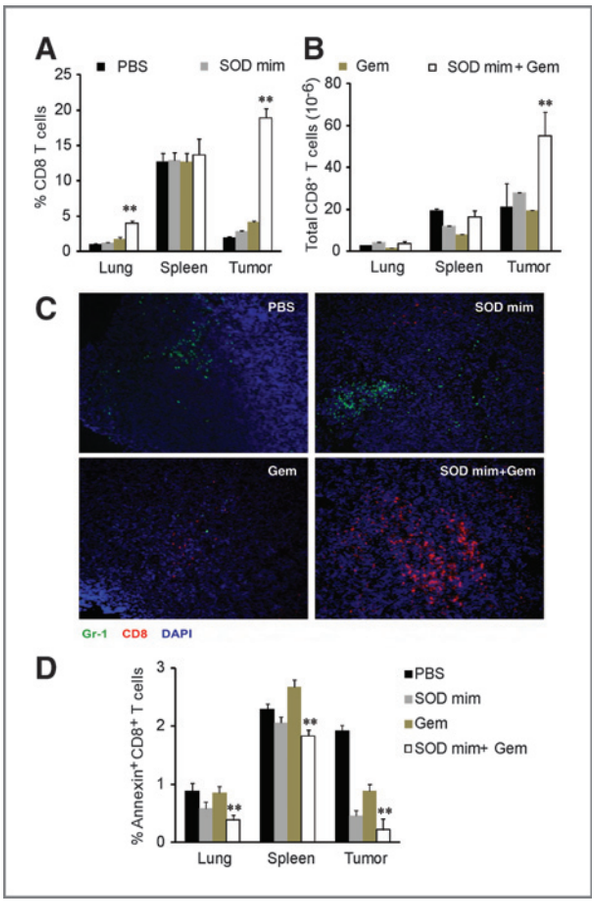

Figure 3. SOD mim + Gem treatment results in enhanced $CD8^+$ T-cell recruitment and diminished presence of MDSC. A, the percentage of $CD8^+$ T cells was determined by flow-cytometric analyses of cells harvested from lung, spleen, and tumor tissues. Live $CD3^+$ cells in the lymphocyte gate were analyzed for percentage of $CD8^+$ cells. **, $P < 0.01$ when compared with all treatment groups as derived by ANOVA. B, total numbers of $CD8^+$ T cells in lung, spleen, and tumor tissues from each treatment group are presented. C, localization of $Gr\text{-}1^+$ and $CD8^+$ cells as determined by immunofluorescent analyses of OCT frozen tumor tissue stained with anti-Gr-1 and CD8 antibodies. D, percentage $Annexin^+$ $CD8^+$ T cells as determined by flow cytometry of cells harvested from lung, spleen, and tumor tissues. **, $P < 0.001$ in comparison with all other treatment and control groups.

tumor burden (Supplementary Fig. S4A and S4D) and enhanced the memory response (increased percentages of T_{EM}, T_{CM}, and T_{SCM}) to levels noted in the WT mice (Supplementary Fig. S4B and S4C).

Thiol-dependent STAT-3 activation is enhanced in memory cells following combination therapy

Reduction of ROS levels is associated with reduced thiol groups on T-cell surfaces, which contributes to persistence of memory cells and protection from apoptotic cell death (22). T_{CM} are reported to have more reduced thiols as compared with T_{EM} and can withstand oxidative stress (22, 23). Therefore, we hypothesized that $CD8^+$ T cells purified from the combination therapy treated mice may express high levels of thiols and therefore, are more effective in antitumor response. On the basis of maleimide reactivity, an increase in reduced thiols was detected in $CD8^+$ T cells obtained from tumor, spleen, and lungs of mice treated with combination therapy (Fig. 5A; $P < 0.01$ for SOD mim + Gem vs. Gem). Furthermore, phosphorylation of a thiol-dependent transcription factor STAT-3 (24, 25), critical for memory $CD8^+$ T-cell function (26), was in memory cells following combination therapy. As demonstrated by phospho-flow analysis of memory subsets (Fig. 5B), increased levels of phosphorylated STAT-3 were detected in tumor-derived T_{EM} and T_{CM} obtained from mice given combination therapy when compared with gemcitabine therapy alone. In addition, the ratio of p-STAT-3 to total STAT-3 changed significantly in the memory cells as compared with effector cells and the percentage of phosphorylation was enhanced in the combination therapy group as compared with all the other individual treatments (Fig. 5C; $P < 0.05$ for SOD mim + Gem vs. Gem for T_{EM} and T_{CM}). We then investigated whether the combination therapy triggers switching of the metabolic pathways that fuel the energy production required for function of the memory T-cell subsets. LC/MS-MRM analysis of metabolites of these $CD8^+$ T-cell memory subsets (Fig. 5D) indicated that both T_{EM} and T_{CM} subsets from combination therapy had a higher dependency on glycolysis compared with those from individual therapies alone. Thus, the reduction of MDSC infiltration and MDSC-associated ROS altered the metabolic status of these tumor-specific $CD8^+$ T-cell memory subsets.

Targeting MDSC and the ROS pathway enhances polyfunctional activity and the cytotoxic potential of memory $CD8^+$ T cells

We then investigated whether the quality of the $CD8^+$ T-cell response is modulated by the combination therapy. We first compared the cytotoxic potential of these tumor-specific memory $CD8^+$ T-cell subsets. As shown in Fig. 5E, the cytolytic activity of both T_{EM} and T_{CM} derived from tumor tissues of SOD mim + Gem therapy mice was more potent against target lung cancer cells when compared with those obtained from mice receiving individual therapies ($P < 0.05$). The T_{CM} purified from the SOD mim therapy group were also cytolytic. Importantly, the $CD8^+$ T cells purified from mice treated with combination therapy showed an enhancement of the polyfunctional response with increased percentages of IFN-γ, cytoplasmic perforin, and $IL\text{-}2^+$ $CD8^+$ T cells (Fig. 6A–C; $P < 0.01$ for IFN-γ expression; $P < 0.001$ for $perforin^+$ $CD8^+$T cells, and $IL\text{-}2^+$ $CD8^+$ T cells from tumor). Thus, it is likely that the central role of establishing memory response following combination therapy was not only for long-term antitumor immune senescence but also against relapse following long-term remission.

Adoptive transfer of memory $CD8^+$T cells from therapy groups significantly improved long-term survival of mice bearing lung cancer

Because the increased infiltration of the memory $CD8^+$ T cells following combination therapy lowered lung cancer progression, we investigated whether adoptive transfer of these memory cells would improve survival of mice with established

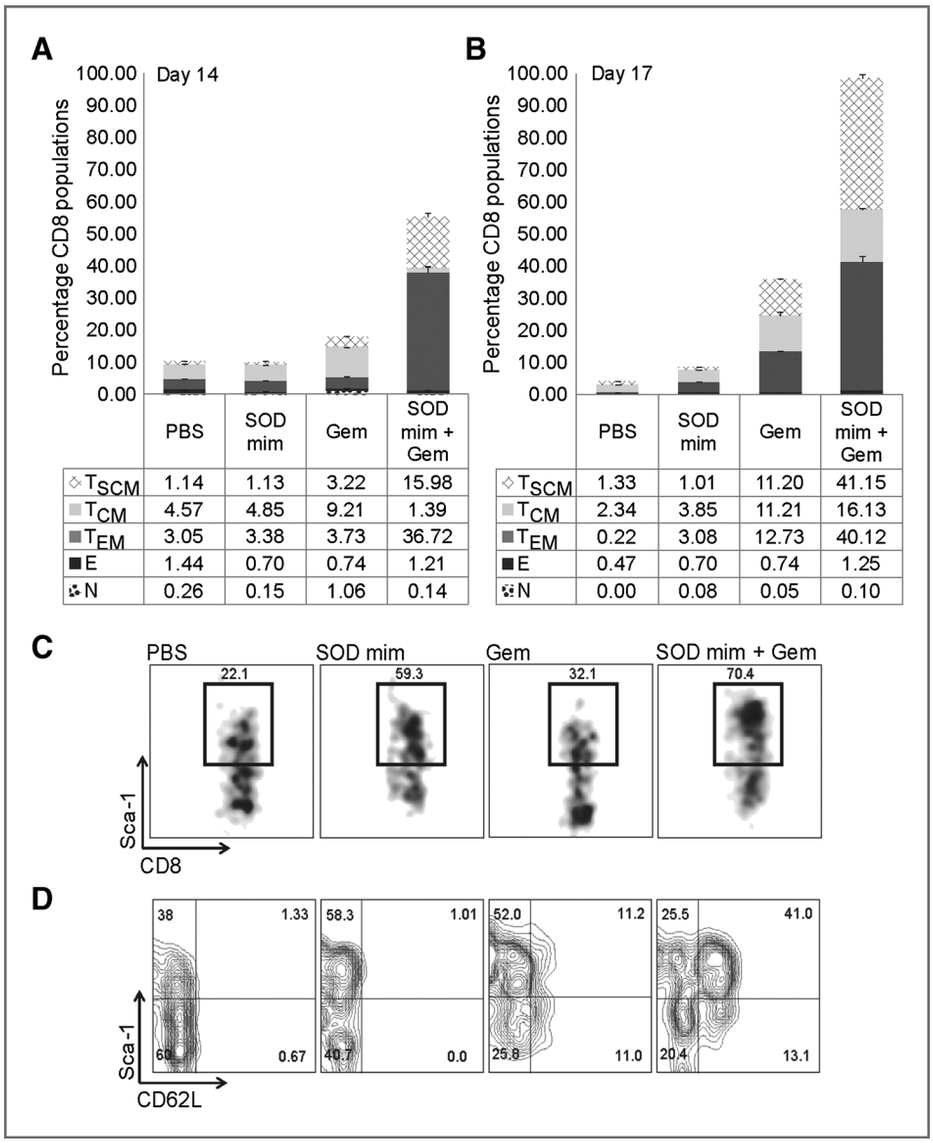

Figure 4. Combination therapy modulates the quantity of the memory $CD8^+$ T-cell response. Stacked histogram plots display percentages of subsets within total $CD8^+$ populations in the tumor tissue at days 14 (A; $P < 0.001$ for SOD mim + Gem versus Gem for T_{EM} and T_{SCM}) and 17. B, $P < 0.01$ for SOD mim + Gem versus Gem for T_{EM} and T_{SCM}; $P < 0.05$ for the same comparison for T_{CM} after establishment of tumor. C, percentage of $CD8^+Sca\text{-}1^+$ T cells in different treatment groups are shown; $P < 0.001$ for SOD mim + Gem compared with Gem and PBS; $P < 0.01$ for SOD mim versus Gem. D, representative FACS plots showing percentage $CD8^+$ T cells that are $Sca\text{-}1^+CD62L^+$, identified as T_{SCM}.

lung tumors. For these studies, effector, T_{CM}, and T_{EM} $CD8^+$ T cells were purified from gemcitabine only and SOD mim + Gem therapy groups and were adoptively transferred into tumor-bearing mice 7 days after lung cancer challenge (Fig. 7A). As shown in Fig. 7B, 80% of mice that received either T_{CM} or T_{EM} from the SOD mim + Gem group survived for up to 80 days after lung cancer challenge as compared with 25-day mean survival of treated mice in control groups ($P < 0.001$ for G+S-E CD8, G+S-T_{CM} CD8, G+S-T_{EM} CD8 and Gem-T_{EM} CD8 compared with PBS group; $P < 0.05$ for PBS group when compared with Gem-E CD8).

Mice that survived for up to 80 days postadoptive transfer were rechallenged with LLC cells to investigate the efficacy of these adoptively transferred memory subsets and their potential to be reactivated in the presence of tumor antigens. Enumeration of circulating memory $CD8^+$ T memory subsets showed a significant increase in the T_{SCM} population in rechallenged mice as compared with the baseline levels (levels of memory cells in adoptive transferred mice before lung cancer rechallenge) and in comparison with tumor challenged control mice (tumor bearing mice without $CD8^+$ T-cell adoptive transfer; Fig. 7C and Supplementary Fig. S5; $P < 0.001$ for T_{SCM} and T_{CM} in rechallenged groups compared with baseline and controls). These persistent memory $CD8^+$ T-cell subsets were efficient in maintaining reduced tumor burden. A reduction in infiltration of MDSC levels was also noted in the adoptive transfer recipients (Fig. 7D and Supplementary Fig. S6; $P < 0.05$ and $P < 0.01$ for T_{CM} compared with T_{EM} and control, respectively). In addition to the increased memory subsets in circulation, congenic adoptive transfer of memory subsets further confirmed the expansion of adoptively transferred $CD8^+$ T-cell memory subsets specifically in the tumor tissue (Supplementary Fig. S7).

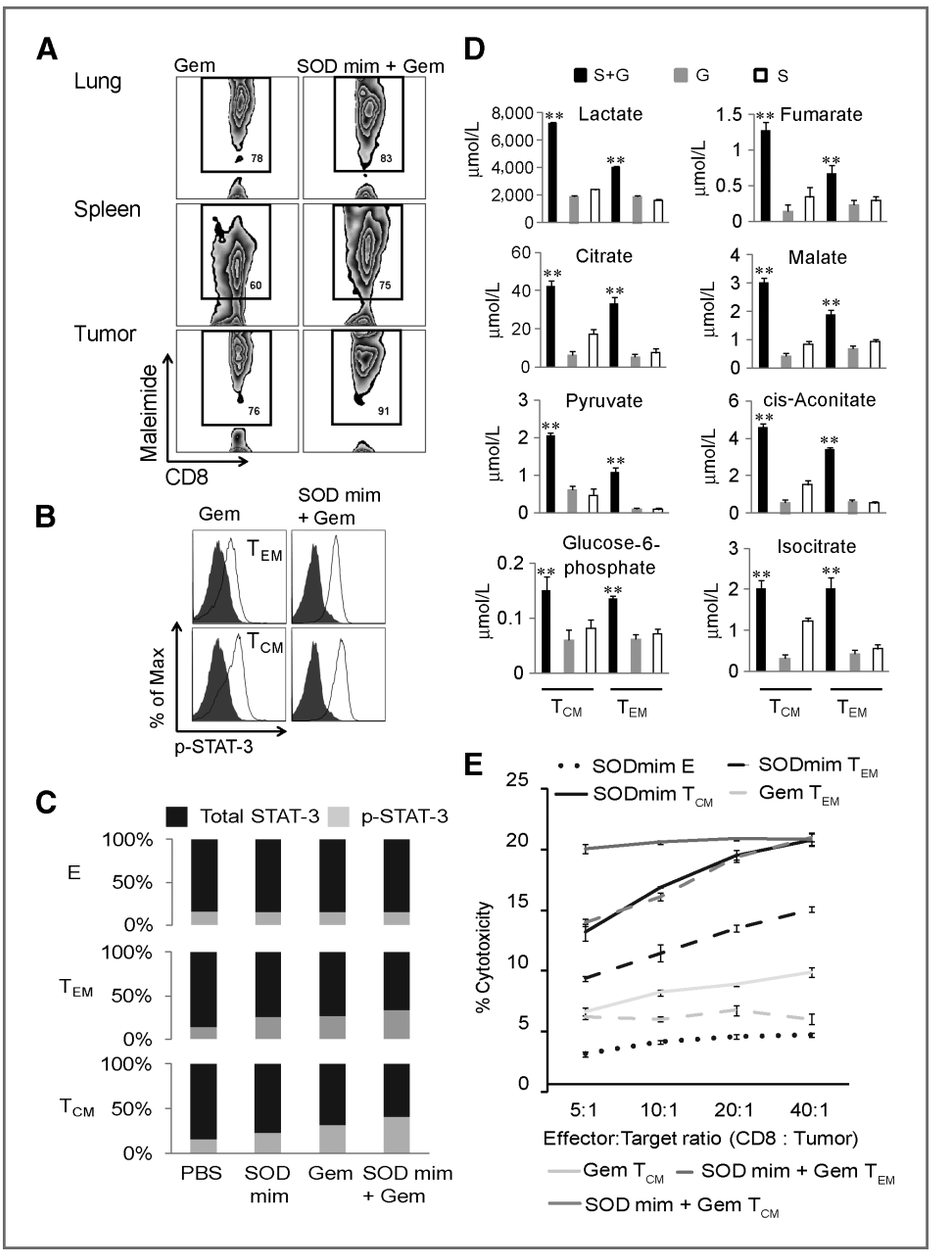

Figure 5. Combination therapy modulates redox-mediated STAT-3 signaling and metabolic switching of memory $CD8^+$ T-cell subsets. A, FACS plots of memory subsets stained with maleimide (detects cell surface thiols) and anti-CD8 antibody; **, $P < 0.01$ for $CD8^+Maleimide^+$ cells in comparison to treatment groups SOD mim + Gem versus Gem for lung, spleen, and tumor tissues ($n = 3$ mice/group, four replicate experiments). B, overlaid histograms of phospho flow-cytometric analyses of T_{EM} and T_{CM} cells from Gem and SOD mim + Gem treatment groups stained with phospho-STAT-3 antibody. Gray tracings, the memory subsets from the SOD mim group. C, stacked plot graphs showing an increased percentage of T_{CM} with p-STAT3 as compared with total STAT-3. D, concentrations of metabolites of glycolysis and Krebs cycle detected in tumor-specific memory $CD8^+$ T-cell subsets analyzed by LC/MS-MRM in SOD mim, Gem, and SOD mim + Gem treatment groups; **, $P < 0.01$ for treatment group S+G (SOD mim + Gem) compared with Gem alone (G) or SOD mim alone (S) for all metabolites. E, cytotoxic activity was significant in $CD8^+$ T cells from mice treated with $CD8^+$ T central memory cells from SOD mim + Gem and from SOD mim alone. The cytotoxicity assay was carried out using a LIVE/DEAD Cell-Mediated Cytotoxicity Kit (Molecular Probes). LLC cells were labeled with $DiOC_{18}$ and incubated for 1 hour with the effector memory $CD8^+$ T-cell subsets at the E:T ratios described in the text. Percentage cytotoxicity was determined by flow-cytometric analysis as described in Materials and Methods; $P < 0.05$ SOD mim + Gem T_{CM} compared with SOD mim + Gem T_{EM}; $P < 0.05$ SOD mim + Gem memory T-cell subsets compared with Gem or SOD mim alone groups ($n = 3$ mice/group; $n = 3$ replicates/group).

Collectively, this study convincingly demonstrates that targeting the proliferation and immunosuppressive functions of MDSC promote antitumor immunity by enhancing the quantity and quality of the $CD8^+$ T-cell responses and promote persistent immunologic memory, thereby reducing tumor burden and prolonging survival of mice with lung cancer.

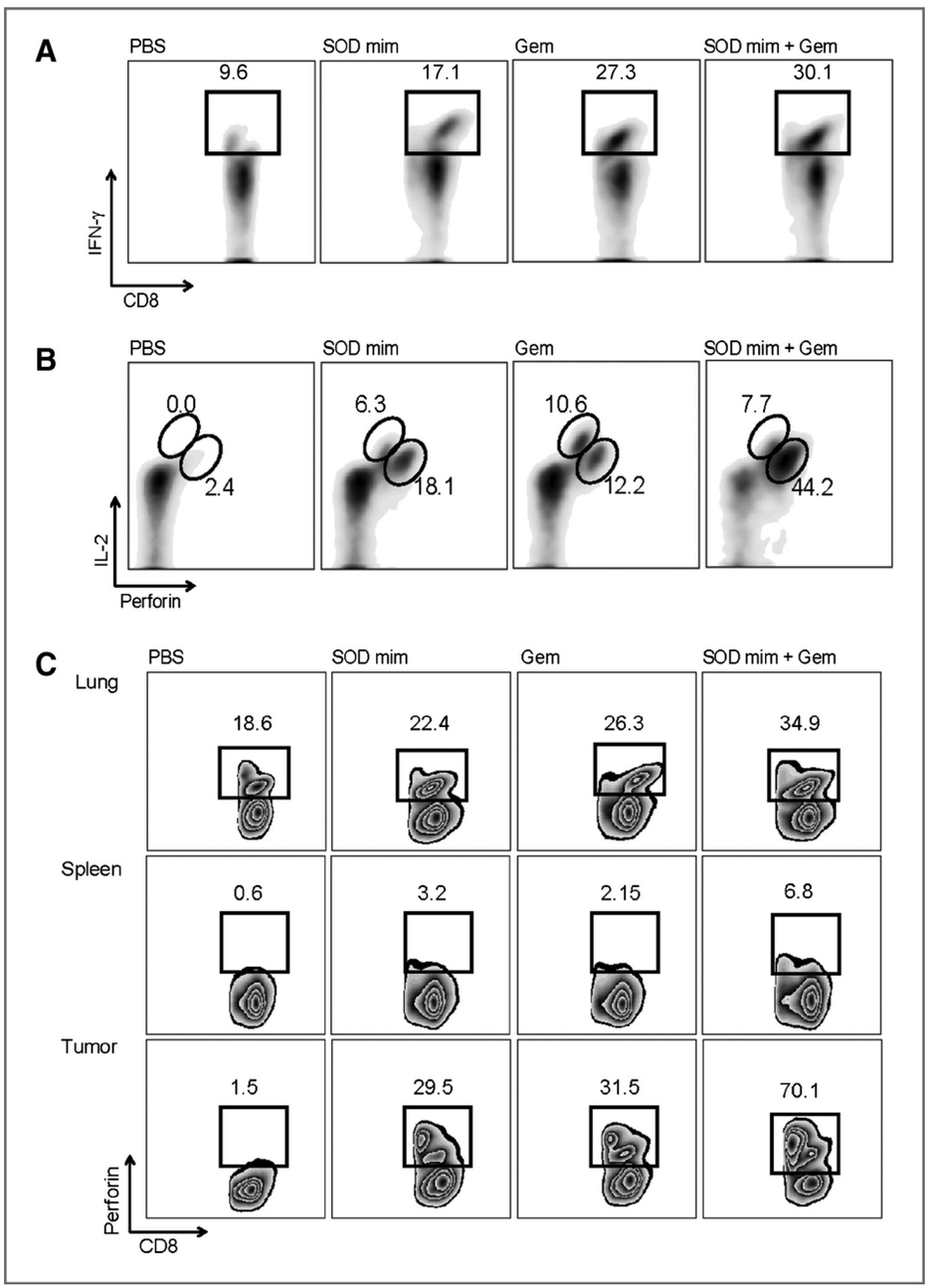

Figure 6. Combination therapy increased the percentage of multifunctional $CD8^+$ T cells producing IFN-γ, IL-2, and perforin. A, FACS plots showing IFN-γ expression in $CD8^+$ $Perforin^+$ T cells in tumor tissue; $P < 0.05$ for comparisons of SOD mim + Gem versus Gem; $P < 0.01$ for comparisons of SOD mim + Gem and Gem versus SOD mim, and for all treatment groups compared with PBS controls ($n = 4$ mice/group, three replicate experiments). B, FACS plots showing the percentage of IL-2–secreting $CD8^+$ $Perforin^+$ T cells in tumor tissue; $P < 0.001$ for SOD mim + Gem compared with Gem or SOD mim alone ($n = 4$ mice/group, three replicate experiments). C, FACS plots of gated $CD8^+$ T cells stained for intracellular expression of perforin in lung, spleen, and tumor tissues of all treatment groups; lung samples: $P < 0.01$ for $CD8^+perforin^+$ cells from the group SOD mim + Gem compared with Gem, SOD mim alone, or PBS controls; spleen samples: $P < 0.05$ for SOD mim + Gem compared with all other treatment groups; tumor samples: $P < 0.001$ for SOD mim + Gem compared with all other treatment groups and PBS controls ($n = 4$ mice/group, three replicate experiments). The percentages displayed on all FACS plots are from a representative run.

Discussion

Recent evidence suggests that immune regulation contributed by MDSC in the TME dampens the long-term efficacy of existing combination chemotherapies for lung cancer (10). ROS produced by MDSC contributes to immunosuppression in the TME (7, 8). MDSC also replenish the tumor stroma with precursors of both TAM and TAN, which contribute to oxidative stress in the TME (27). The multifaceted impact of oxidative stress in the TME is reflected not only in the impairment of T cell and natural killer (NK) cell activity, but also on redox-mediated regulation of T-cell signaling and T-cell survival (22, 28). The differentiation state of the lymphocytes determines their function and persistence (29, 30). Mechanisms that modulate survival and function of T-cell subsets, particularly in regard to their differential sensitivity to oxidative stress in the TME, have yet to be completely elucidated. This is of great relevance in the context of memory $CD8^+$ T cells, which are a critical component of protective immunity against cancer. Differential sensitivity of memory cell phenotypes to oxidative stress may skew the memory repertoire to a particular subset, leading to its persistence in TME. Therefore,

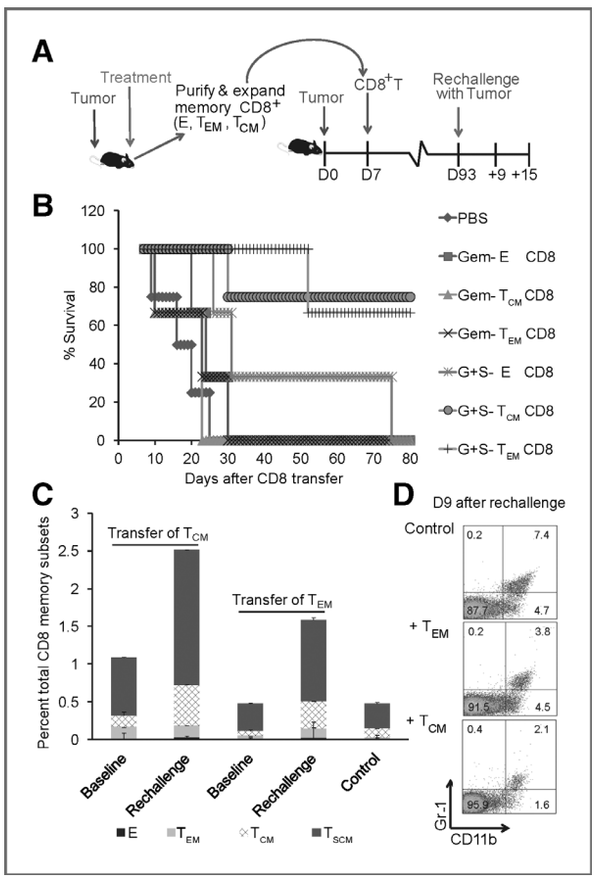

Figure 7. Central and effector memory CD8$^+$ subsets from mice treated with combination therapy efficiently targets tumor cells and prolongs survival following adoptive therapy. A, schematic showing the time line of adoptive transfer and tumor rechallenge. B, a Kaplan–Meier survival curve showing an increase in percentage survival of mice with established lung cancer after intravenous adoptive transfer with 10^5 indicated memory CD8$^+$ T-cell subsets ($n = 4$–6 mice/group). Data shown are cumulative results from two independent experiments with 5 mice/group and analyzed by Mantel–Cox log-rank test ($P < 0.05$ for PBS versus Gem-E CD8; $P < 0.05$ for PBS versus Gem-T_{EM} CD8; $P < 0.001$ for PBS versus G+S-E CD8; $P < 0.001$ for PBS versus G+S-T_{CM} CD8; and $P < 0.001$ for PBS versus G+S- T_{EM} CD8). C, stacked histogram depicting the percentage of total CD8$^+$ memory subsets at baseline and at day 9 after rechallenge with tumor in adoptive transfer recipient mice with T_{CM} or T_{EM} transfer ($n = 3$ mice/group, two replicate experiments; $P < 0.001$ for T_{SCM} and T_{CM} in rechallenged groups compared with baseline and controls. D, FACS plots of circulating Gr-1$^+$ CD11b$^+$ MDSC at day 9 after rechallenge in adoptive transfer recipients compared with tumor challenged controls; $P < 0.05$ T_{CM} compared T_{EM} and $P < 0.01$ T_{CM} compared with controls ($n = 3$ mice/group, two replicate experiments). The percentages displayed on FACS plots are from a representative run.

strategies that eliminate MDSC-mediated immunosuppression in combination with antioxidant therapeutics to enhance the CD8$^+$ T-cell effector and memory response may be efficacious as novel anti-lung cancer regimens.

In this study, we provide evidence that gemcitabine when used in combination with an SOD mim, result in successful inhibition of MDSC, Treg, and TAN infiltration and a significant reduction of ROS in the TME (Fig. 2). Inhibition of MDSC observed with this therapy is supported by recent studies that demonstrate efficacy of chemotherapeutic strategies in targeting MDSC (31–33). The observed reduction of infiltration of Treg is consistent with depletion of MDSC, as MDSCs induce development (34) and promote migration and recruitment of Treg to sites of chronic inflammation (35). The reduction in neutrophils observed in the tumor tissue following combination therapy is consistent with the reduction in MDSC, as MDSC infiltration have been associated with increased TAN in the TME. The enhanced percentages and absolute numbers of CD8$^+$ T cells and reduction in their apoptotic death following combination therapy (Fig. 3) suggest a potential utility of this approach for reducing tumor burden and stimulating antitumor immunity by providing an ideal microenvironment for optimal T-cell function.

Our novel observation that the combination therapy enhances both the quantity and quality of the memory response with polyfunctional and cytolytic activity, all support the potential of this strategy to promote T-cell survival and function (Figs. 4 and 5). In an MDSC- and ROS-depleted environment, the memory response to tumor challenge were skewed toward T_{CM}, T_{EM}, and more interestingly, a subset T_{SCM} with a stem cell memory phenotype (Fig. 4). Similar observations noted with MDSC depletion using anti-Gr-1 Ab and SOD mim further validates these findings. T_{SCM} CD8$^+$ T cells have extensive replicative potential *in vivo* and maintain the naïve CD44$^-$CD62L$^+$ phenotype (30). These cells display the glycosylphosphatidyl inositol-linked molecule Sca-1, a marker for self-renewing cells (22, 29). Our studies showed a significant early increase in T_{EM} and T_{SCM} phenotypes followed by a shift in the expansion of both T_{CM} and T_{SCM} (Fig. 4) as a late response to combination therapy. It is possible that redox regulation by MDSC may cause an intrinsic defect in the ability of T_{EM} and T_{CM} to proliferate in response to tumor challenge and this defect could be reversed or rectified by depletion of MDSC and associated ROS in the TME. Oxidative stress in the TME may also affect the differentiation pathways of these memory subsets and skew the memory repertoire toward subsets that are less sensitive to oxidative stress such as the T_{CM} and T_{EM} (22, 28). Depletion of ROS and MDSC from TME could then trigger the expansion of these resistant memory cell subsets, as well as T_{SCM} (stem cell phenotype with high proliferative capacity). Consistent with these possibilities, our data suggest that combination therapy-based depletion of the excess ROS and MDSC enhanced the CD8$^+$ T-cell memory response, consistently skewing the memory repertoire to T_{CM} and T_{EM} cells, and increased numbers of T_{SCM} (Fig. 4). These observations were also noted in catalase-deficient mice (Supplementary Fig. S4). Our studies do not, however, delineate whether alterations in differentiation pathways of these T-cell subsets account for the observed cellular redistribution in the memory compartment.

SOD mims are effective free radical scavengers in many disease models including those of stroke (36), diabetes (37), and sickle cell anemia (38). They have been shown to protect normal tissues against radiation-induced damage presumably by alleviating oxidative stress (39). In addition, there is mounting evidence that SOD mims may enhance tumor

radioresponsiveness (40, 41) Although the SOD mim, which we have used in our combination therapy, does not enhance tumor responsiveness to chemotherapy, it offers significant advantages for adoptive cell therapy strategies as it enhances persistent antitumor immunity.

Our data suggest that modulation of redox regulation and signaling by gemcitabine and combination therapy may impact long-lived memory populations. We show that lowered oxidative stress in the TME, resulting from depletion of MDSC and ROS, is associated with an increased number of cell surface thiols on T_{CM} (Fig. 5). This is consistent with earlier reports that memory subsets resistant to activation induced cell death or apoptosis have increased thiols contributing to their persistence (22, 29). We do not anticipate any direct effects of SOD mim on thiols, but rather the combination therapy modulates upstream events, resulting in a change in the redox status of the memory cells. The modulation of reduced thiols on T-cell surface may reduce the threshold for T-cell activation and enhanced their proliferative capacity *in vivo*. The observed increase in phosphorylation of thiol-dependent STAT-3 in T_{CM} as compared with T_{EM} (Fig. 5B and C), may allow them to persist as memory cells, as STAT-3 activation is critical for maintenance of long-term memory (26).

Because metabolism underlies the functional capacity of T cells, their maintenance and their persistence during an immune response, therapeutic strategies that manipulate the T-cell metabolism may alter the outcome of the antitumor response (42). This is particularly relevant in our observations that the combination therapy not only enhanced the $CD8^+$ memory T-cell response, but also modulated the metabolism of T_{CM} and T_{EM} subsets. These memory cells were glycolysis-dependent and relied on a more readily available ATP source than those resulting from individual therapies (Fig. 5D). These observations are also consistent with the association of STAT-3 activation and persistence of T_{CM} and T_{EM} subsets in adoptive transfers and rechallenges with tumor cells. T_{CM} and T_{EM} subsets from combination therapy responded quickly and vigorously to the tumor rechallenge compared with controls. Adoptive transfer recipients of T_{CM} purified from combination therapy–treated mice were more efficient than T_{EM} in eradicating tumor burden and prolonging survival (Fig. 7). In addition, rechallenging the surviving animals with a second round of tumor cells produced an increased expansion of T_{CM} as compared with T_{EM}, successful eradication of tumor burden, and a reduced infiltration of MDSC (Fig. 7). We have not delineated, however, whether the changes in the metabolic program of $CD8^+$ memory T-cell subsets triggered by combination therapy is to either increase energy production to cope with the increased demand to proliferate, to provide biosynthetic precursors or to generate reducing equivalents to balance the change in redox status in the TME.

We have not investigated the efficacy of these memory cells after repeated exposure to the antigen or their efficiency in targeting tumor cells following repeated cycles of adoptive transfer. In addition, we have not addressed the potential of this strategy for small cell lung cancer, cancers other than lung cancers, and/or other cancers that metastasize to the lung. Nevertheless, our investigations certainly suggest that depletion of MDSC and ROS may provide a preferential advantage for T_{CM} to be more functionally active, proliferative, and persistent to provide long-term immunity against lung cancer.

This is particularly relevant for adoptive cell transfer therapies that are being tested in early-stage clinical trials for advanced cancer. There is also an impending need for novel effective approaches to generate persistent immunity in patients in whom the potential for complete elimination of tumor antigens are highly unlikely. Therefore, defining determinants for successful $CD8^+$ T-cell adoptive immunotherapy are essential. Our combination therapy offers an attractive strategy for adoptive T-cell therapy in that it has potential to generate long-lived populations of T_{CM} equipped with the dual potential of both immune surveillance, as well as tumor eradication. In addition, this therapeutic strategy enhances memory cells with a self-renewing phenotype that may increase their long-term efficacy and persistence. We believe there is a potential role for this combination therapy as an adjuvant therapy in treatment strategies to eradicate early lung cancer and has implications for prevention of lung cancer relapse or recurrence.

Disclosure of Potential Conflicts of Interest

No potential conflicts of interest were disclosed.

Authors' Contributions

Conception and design: A. Sawant, S. Ponnazhagan, J.S. Deshane
Development of methodology: A. Sawant, S. Ponnazhagan, J.S. Deshane
Acquisition of data (provided animals, acquired and managed patients, provided facilities, etc.): A. Sawant, H.M. Tse, J. Roth, S. Ponnazhagan, J.S. Deshane
Analysis and interpretation of data (e.g., statistical analysis, biostatistics, computational analysis): A. Sawant, C.C. Schafer, J. Zmijewski, V.J. Thannickal, S.C. Grant, S. Ponnazhagan, J.S. Deshane
Writing, review, and/or revision of the manuscript: A. Sawant, C.C. Schafer, J. Zmijewski, J. Roth, G.P. Siegal, V.J. Thannickal, S.C. Grant, S. Ponnazhagan, J.S. Deshane
Administrative, technical, or material support (i.e., reporting or organizing data, constructing databases): C.C. Schafer, T.H. Jin, J. Zmijewski, Z. Sun, G.P. Siegal, S. Ponnazhagan, J.S. Deshane
Study supervision: S. Ponnazhagan, J.S. Deshane

Acknowledgments

The authors thank Doyle Ray Moore and Dr. Stephen Barnes of the Targeted Metabolomics and Proteomics Laboratory, UAB for the metabolomic analyses included in this study. The authors also thank Marion Spell (Center for AIDS Research Flow Facility Core for cell sorting) and Enid Keyser (Rheumatic Diseases Analytic and Preparative Cytometry Facility) for their technical support for fluorescence-activated cell sorting (FACS).

Grant Support

This study was supported by the Collaborative Development Grant for Immunology and Cancer Immunotherapeutics funded by the National Cancer Institute (NCI CA13148-39 to J.S. Deshane and S. Ponnazhagan), R01CA132077 and R01CA133737 to S. Ponnazhagan. Funds for the operation of the Targeted Metabolomics and Proteomics Laboratory come in part from the UAB Center for Nutrient-Gene Interaction (U54 CA 100949), the Purdue-UAB Botanicals Center for Age-Related Disease (P50 AT00477), the UAB O'Brien Acute Kidney Injury Center (P30 DK079337), the UAB Skin Disease Research Center (P30 AR50948), and the UAB Lung Health Center.

The costs of publication of this article were defrayed in part by the payment of page charges. This article must therefore be hereby marked *advertisement* in accordance with 18 U.S.C. Section 1734 solely to indicate this fact.

Received April 9, 2013; revised August 21, 2013; accepted September 9, 2013; published OnlineFirst October 1, 2013.

References

1. Society AC. Cancer facts and figures 2012. Atlanta, GA: American Cancer Society; 2012.
2. Howlader N, Noone AM, Krapcho M, Neyman N, Aminou R, Altekruse SF, et al. SEER cancer statistics review. Bethesda, MD: U.S. National Institutes of Health, National Cancer Institute; 1973–2008.
3. William WN Jr, Glisson BS. Novel strategies for the treatment of small-cell lung carcinoma. Nat Rev Clin Oncol 2011;8:611–9.
4. Lawless MW, O'Byrne KJ, Gray SG. Targeting oxidative stress in cancer. Expert Opin Ther Targets 2010;14:1225–45.
5. Dougan M, Li D, Neuberg D, Mihm M, Googe P, Wong KK, et al. A dual role for the immune response in a mouse model of inflammation-associated lung cancer. J Clin Invest 2011;121:2436–46.
6. Vacchelli E, Galluzzi L, Rousseau V, Rigoni A, Tesniere A, Delahaye N, et al. Loss-of-function alleles of P2RX7 and TLR4 fail to affect the response to chemotherapy in non–small cell lung cancer. Oncoimmunology 2012;1:271–8.
7. Gabrilovich DI, Ostrand-Rosenberg S, Bronte V. Coordinated regulation of myeloid cells by tumours. Nat Rev Immunol 2012;12:253–68.
8. Ostrand-Rosenberg S. Myeloid-derived suppressor cells: more mechanisms for inhibiting antitumor immunity. Cancer Immunol Immunother 2010;59:1593–600.
9. Gabrilovich DI, Nagaraj S. Myeloid-derived suppressor cells as regulators of the immune system. Nat Rev Immunol 2009;9:162–74.
10. Srivastava MK, Andersson A, Zhu L, Harris-White M, Lee JM, Dubinett S, et al. Myeloid suppressor cells and immune modulation in lung cancer. Immunotherapy 2012;4:291–304.
11. Mundy-Bosse BL, Lesinski GB, Jaime-Ramirez AC, Benninger K, Khan M, Kuppusamy P, et al. Myeloid-derived suppressor cell inhibition of the IFN response in tumor-bearing mice. Cancer Res 2011;71:5101–10.
12. Deshane J, Zmijewski JW, Luther R, Gaggar A, Deshane R, Lai JF, et al. Free radical-producing myeloid-derived regulatory cells: potent activators and suppressors of lung inflammation and airway hyperresponsiveness. Mucosal Immunol 2011;4:503–18.
13. Chun SH, Lee JE, Park MH, Kang JH, Kim YK, Wang YP, et al. Gemcitabine plus platinum combination chemotherapy for elderly patients with advanced non–small cell lung cancer: a retrospective analysis. Cancer Res Treat 2011;43:217–24.
14. Suzuki E, Kapoor V, Jassar AS, Kaiser LR, Albelda SM. Gemcitabine selectively eliminates splenic Gr-1^+/CD11b^+ myeloid suppressor cells in tumor-bearing animals and enhances antitumor immune activity. Clin Cancer Res 2005;11:6713–21.
15. Le HK, Graham L, Cha E, Morales JK, Manjili MH, Bear HD. Gemcitabine directly inhibits myeloid derived suppressor cells in BALB/c mice bearing 4T1 mammary carcinoma and augments expansion of T cells from tumor-bearing mice. Int Immunopharmacol 2009;9:900–9.
16. Batinic-Haberle I, Spasojevic I, Tse HM, Tovmasyan A, Rajic Z, St Clair DK, et al. Design of Mn porphyrins for treating oxidative stress injuries and their redox-based regulation of cellular transcriptional activities. Amino Acids 2012;42:95–113.
17. Batinic-Haberle I, Reboucas JS, Spasojevic I. Superoxide dismutase mimics: chemistry, pharmacology, and therapeutic potential. Antioxid Redox Signal 2010;13:877–918.
18. Facciabene A, Motz GT, Coukos G. T-regulatory cells: key players in tumor immune escape and angiogenesis. Cancer Res 2012;72:2162–71.
19. Kennedy BC, Shimato S, Anderson RC, Bruce JN. Defining the mechanisms of CD8 T-cell tumor tolerance. Immunotherapy 2011;3:23–26.
20. Apetoh L, Vegran F, Ladoire S, Ghiringhelli F. Restoration of anti-tumor immunity through selective inhibition of myeloid derived suppressor cells by anticancer therapies. Curr Mol Med 2011;11:365–72.
21. Yu XZ, Anasetti C. Memory stem cells sustain disease. Nat Med 2005;11:1282–3.
22. Mehrotra S, Mougiakakos D, Johansson CC, Voelkel-Johnson C, Kiessling R. Oxidative stress and lymphocyte persistence: implications in immunotherapy. Adv Cancer Res 2009;102:197–227.
23. Takahashi A, Hanson MG, Norell HR, Havelka AM, Kono K, Malmberg KJ, et al. Preferential cell death of $CD8^+$ effector memory ($CCR7^-CD45RA^-$) T cells by hydrogen peroxide-induced oxidative stress. J Immunol 2005;174:6080–7.
24. Wang Y, Ma X, Yan S, Shen S, Zhu H, Gu Y, et al. 17-hydroxy-jolkinolide B inhibits signal transducers and activators of transcription 3 signaling by covalently cross-linking Janus kinases and induces apoptosis of human cancer cells. Cancer Res 2009;69:7302–10.
25. Xie Y, Kole S, Precht P, Pazin MJ, Bernier M. S-glutathionylation impairs signal transducer and activator of transcription 3 activation and signaling. Endocrinology 2009;150:1122–31.
26. Siegel AM, Heimall J, Freeman AF, Hsu AP, Brittain E, Brenchley JM, et al. A critical role for STAT3 transcription factor signaling in the development and maintenance of human T cell memory. Immunity 2011;35:806–18.
27. Peden DB. The role of oxidative stress and innate immunity in O(3) and endotoxin-induced human allergic airway disease. Immunol Rev 2011;242:91–105.
28. Nakamura K, Yube K, Miyatake A, Cambier JC, Hirashima M. Involvement of CD4 D3-D4 membrane proximal extracellular domain for the inhibitory effect of oxidative stress on activation-induced CD4 down-regulation and its possible role for T cell activation. Mol Immunol 2003;39:909–21.
29. Sallusto F, Geginat J, Lanzavecchia A. Central memory and effector memory T cell subsets: function, generation, and maintenance. Annu Rev Immunol 2004;22:745–63.
30. June CH. Principles of adoptive T cell cancer therapy. J Clin Invest 2007;117:1204–12.
31. Lu T, Ramakrishnan R, Altiok S, Youn JI, Cheng P, Celis E, et al. Tumor-infiltrating myeloid cells induce tumor cell resistance to cytotoxic T cells in mice. J Clin Invest 2011;121:4015–29.
32. Tongu M, Harashima N, Monma H, Inao T, Yamada T, Kawauchi H, et al. Metronomic chemotherapy with low-dose cyclophosphamide plus gemcitabine can induce anti-tumor T cell immunity *in vivo*. Cancer Immunol Immunother 2013;62:383–91.
33. Sim SH, Ahn YO, Yoon J, Kim TM, Lee SH, Kim DW, et al. Influence of chemotherapy on nitric oxide synthase, indole-amine-2,3-dioxygenase and CD124 expression in granulocytes and monocytes of non–small cell lung cancer. Cancer Sci 2012;103:155–60.
34. Pan PY, Ma G, Weber KJ, Ozao-Choy J, Wang G, Yin B, et al. Immune stimulatory receptor CD40 is required for T-cell suppression and T regulatory cell activation mediated by myeloid-derived suppressor cells in cancer. Cancer Res 2010;70:99–108.
35. Bronte V, Zanovello P. Regulation of immune responses by L-arginine metabolism. Nat Rev Immunol 2005;5:641–54.
36. Shimizu K, Rajapakse N, Horiguchi T, Payne RM, Busija DW. Protective effect of a new nonpeptidyl mimetic of SOD, M40401, against focal cerebral ischemia in the rat. Brain Res 2003;963:8–14.
37. Haskins K, Bradley B, Powers K, Fadok V, Flores S, Ling X, et al. Oxidative stress in type 1 diabetes. Ann N Y Acad Sci 2003;1005:43–54.
38. Kaul DK, Liu XD, Zhang X, Ma L, Hsia CJ, Nagel RL. Inhibition of sickle red cell adhesion and vasoocclusion in the microcirculation by antioxidants. Am J Physiol Heart Circ Physiol 2006;291:H167–175.
39. Vujaskovic Z, Batinic-Haberle I, Rabbani ZN, Feng QF, Kang SK, Spasojevic I, et al. A small molecular weight catalytic metalloporphyrin antioxidant with superoxide dismutase (SOD) mimetic properties protects lungs from radiation-induced injury. Free Radic Biol Med 2002;33:857–63.
40. Moeller BJ, Batinic-Haberle I, Spasojevic I, Rabbani ZN, Anscher MS, Vujaskovic Z, et al. A manganese porphyrin superoxide dismutase mimetic enhances tumor radioresponsiveness. Int J Radiat Oncol Biol Phys 2005;63:545–52.
41. Gridley DS, Makinde AY, Luo X, Rizvi A, Crapo JD, Dewhirst MW, et al. Radiation and a metalloporphyrin radioprotectant in a mouse prostate tumor model. Anticancer Res 2007;27:3101–9.
42. van der Windt GJ, Pearce EL Metabolic switching and fuel choice during T-cell differentiation and memory development. Immunol Rev 2012;249:27–42.